Investigating the Accuracy of Digital Image Correlation in Monitoring Strain Fields across Historical Tapestries

Nwanoro, K.C[1*], Harrison, P.[2] and Lennard, F.[3]

[1*] Department of Chemistry, Lancaster University, Lancaster, UK

[2]School of Engineering, University of Glasgow, Glasgow, UK

[3] School of Culture and Creative Arts, University of Glasgow, Glasgow, UK

Abstract

Finite element generated synthetic image deformation is used to assess factors affecting the reliability and accuracy of strain fields measured by the DIC technique, when using the inherent historical tapestry image to track deformations. Compared with direct correlation with the reference image, incremental correlation is found to introduce accumulated error and is less suitable for DIC analysis under low strains. Image quality, for example variation in resolution, is demonstrated to strongly affect DIC performance. Finally, it is recommended that an iterative approach is required to determine the optimum subset and strain filter size for effective DIC analysis using inherent tapestry patterns, especially at low strain levels.

Keywords: Digital image correlation, finite element analysis, Full-field strain measurement, Tapestry monitoring.

1. Introduction

The use of highly accurate techniques of digital image correlation (DIC) [1] for full-field strain measurement and experimental analysis of fluid, biomechanical and mechanical structures and components is very common and well established. Because DIC is a noncontact surface strain measurement technique, it is commonly used in monitoring full-field strain and deformation across delicate heritage paintings [2-4] and historical tapestries [5-10]. The previous studies using DIC for strain monitoring of historical tapestries focused on the measurement of strain distributions across tapestries under self-weight loading conditions, using the tapestry's inherent image to track deformation; the usual application of a speckle pattern [11] on the specimen surface is not feasible with historic artefacts. Monitoring strain and deformation across panel paintings using their natural texture as DIC tracking information has been found to be less effective [3]. To improve the performance of DIC measurement across panel paintings, removable mark trackers are placed strategically across the painting panel surface. [3,4] Due to the physical condition, size, weight and position of historical tapestries in historic houses and museums, using such mark trackers for DIC in-situ strain monitoring is not feasible and the only tracking information is often the fabrics' inherent texture. Extensive research on DIC performance assessment techniques [11-16] has shown that in the context of normal materials and structures, the quality, density, size and randomness of speckle pattern applied on the test sample surface are fundamental factors that determine the accuracy and reliability of the DIC measurement results. In the absence of ideal speckle pattern in using DIC techniques for full-field strain monitoring across historical tapestries inevitably leads to greater uncertainty in the experimental DIC-derived strain measurements; hence a robust method is required to determine the viability and reliability of using DIC when using the tapestry's image and texture to track

surface strains. As a continuation of Alsayednoor et al. [17], analysis tools have been further developed to aid conservators and conservation scientists determine the viability, accuracy and reliability of using DIC with tapestries, using the inherent tapestry image to track displacements. The analysis tools have the ability to determine the accuracy, potential sources of error and reliability of DIC measurements for any given tapestry image, by comparing the measured DIC results with a known finite element analysis (FEA)-generated synthetic representative deformation field. The analysis tools can be used to verify the viability of the DIC method for any given tapestry image and image quality, prior to carrying out actual experiments.

The accuracy of DIC strain measurements depends on numerous factors. Some are decided by the user in the DIC settings (see Table 2) relating to DIC algorithm accuracy, some are determined during the actual monitoring process and depend on issues such as image acquisition process like camera settings and lighting conditions (see Table 3), others depend on the suitability of the target image (see Table 4) for DIC-based tracking of displacements. In [17], the influence of just the subset size was explored, though many other sensitivity studies are possible including not just the DIC algorithm settings but also the image quality and even the FEA parameters such as mesh density/spatial resolution used to generate the synthetic deformation. Indeed, the only parameter that remains fixed is the suitability of the target image, i.e. the inherent tapestry image is a fixed constraint.

The user's choice of DIC settings and parameter values as well as the acquired image quality can significantly affect the accuracy of DIC measurements. The systematic approach developed in [17] and the current work provides a method for tapestry conservators using DIC techniques for strain monitoring, to determine optimum DIC parameters for optimised strain measurements prior to actual testing. Also, an approach to quantify error associated with DIC full field measurement using local strain maps is introduced considering image quality and DIC settings. Since the actual strain level experienced by tapestries in historical houses and museums is less than the strain level used in the previous study [17], the present investigation examines the influence of DIC parameters, tapestry image quality and numerical approximation techniques, used in developing the DIC viability evaluation tool, at low strain levels. This study provides not only awareness to tapestry conservators on the effects of tapestry image quality and DIC parameters on the accuracy of full-field strain predicted by DIC techniques but also a means of validating DIC measurements, when using tapestry images to track deformation. In this paper, FEA generated synthetic image deformation is used to study factors affecting the accuracy of the DIC technique. Different tapestries of varying size and image complexity are examined both under an imposed displacement and under self-weight loading. The resulting full-field strain map is used to evaluate the full-field DIC accuracy instead of using the average global strain that has been commonly used in previous tapestry strain monitoring studies [7-10] (average global strain is less sensitive to noise, especially at low strain levels). In doing so, the accuracy of DIC using a given tapestry image, under different deformation levels and image quality can be assessed. Guidelines for improving the accuracy of DIC when using inherent tapestry patterns, across a broad range of deformation levels are sought.

The remainder of this paper is structured as follows: in Section 2, the overall methodology adopted in this work including the error assessment methods, DIC settings and the details of the historic tapestries and case studies investigated in this work are presented. The numerical techniques and modelling details including numerical deformation of digital images using

synthetic deformation field generated, material properties, loading and boundary conditions are presented in Section 3. In Section 4, the results and discussions are presented while the overall conclusions are presented in Section 5.

2. Method

Known synthetic heterogeneous deformation fields generated by FEA are used to incrementally deform the original/reference (undeformed) tapestry image. The load magnitude (either a known displacement or weight) is progressively applied using load steps in the FEA and the deformation level at each load step is used to generate a deformed digital image corresponding to that deformation level. Therefore, the number of generated deformed images corresponds to the total number of output steps from the FEA analysis. The procedure for numerical deformation of digital images using a known deformation field generated by FEA is well-documented. The pixel and subpixel locations in a corresponding finite element are displaced using the nodal displacement values through bicubic interpolation. More details of this approach and schematic representation can be found in [12] and further description is not repeated here. DIC software is then used to track the displacements and subsequently calculate the strains occurring across the numerically deformed images. The heterogeneous strain fields occurring in loaded tapestries are related to their complex meso-structure, which results from their manufacture; tapestries are often woven using multiple materials, such as silk and wool. Structural discontinuities occur at boundaries between regions of different colour where stitching is used to join the different regions to maintain the tapestry's integrity. To differentiate and identify different materials and regions in a tapestry image, an edge detection algorithm has been used to identify these colour boundaries, different material properties are assigned to stitching at these boundaries in the FEA simulations in order to generate a representative heterogeneous deformation field. [17].

2.1 Error Assessment

In many DIC analysis software packages, correlation accuracy is commonly used for DIC algorithm performance and error assessment, for example in [18], correlation accuracy is measured in terms of sigma level (in pixel) and provides the confidence interval in matchability between the reference and deformed images for each iteration of the algorithm. Correlation accuracy is how well the subsets are matched during the correlation analysis and depends on some thresholding parameters such as projection errors (epipolar projection), confidence interval and matchability to either retain, adjust or remove data points (subsets) during the correlation analysis. While these metrics might be essential to the convergence of DIC algorithms (achieving correlation criteria) and to some extent valid for displacement error assessment, this does not translate to the error associated with the strain measurement using subset based DIC techniques. This is because the approach for computing strain in subset-based DIC analysis is different from the displacement estimation approach. To compute the strain, two approaches are commonly used; one method is to use a strain filter (with defined data points) to filter the strain computed from the subset-based DIC algorithms, which are sensitive and highly prone to noise, using smoothing algorithms such as Gaussian filtering and weighting functions. The strain filter size acts like a strain gauge size used in the strain calculation. A small strain filter size will produce more localised and higher resolution strains, capturing intricate heterogeneity in complex strain fields. On the other hand, a large strain filter includes more data points in the strain averaging and tends to produce a higher global accuracy but lower

resolution of measured strain field. A second method is to use a strain window approach and a least squares plane fit on subset displacement computed from the DIC analysis [19]. Hence the accuracy and spatial resolution of the strain field computed from DIC depends on the filter size in the first method and window size in the second method. Therefore, using the correlation accuracy as an approach to determine the accuracy of DIC algorithms and settings in strain measurement is not adequate because of potential additional noise resulting from the numerical differential used in the strain computation and could result to inaccurate strain measurement that often leads to lack of confidence in DIC results, especially for historical tapestries and paintings where random speckle patterns cannot be implemented to enhance tracking. To systematically assess the performance of DIC in strain measurement, other approaches are often considered.

2.1.1 Average Global Error Assessment

One approach used to validate DIC measurements has been to compare the global average strain measured using DIC with values obtained from other methods such as strain gauge and optical fibre point measured values [7-10]. Using DIC, the global average strain in any given Region of Interest (ROI) is calculated as the sum of the strains across all pixels in the ROI, divided by the number of pixels. These studies, though pioneering the use of DIC in monitoring and predicting complex strain distributions across historic tapestries, do not assess full-field strain maps, which are one of the main measurement goals for informing conservation and preservation strategies.

2.1.2 Full-field error assessment

Full-field error assessment is performed by comparing the measured DIC and known FEA strain fields. This approach of numerically deforming digital images for the purpose of DIC error quantification is well known and has been implemented in various studies. [11-14,17] By using FEA generated strain fields to deform digital images, error related to the DIC equipment setup such as calibration, misalignment, out of plane displacement and vibration as well as error due to image acquisition during tests are all eliminated and errors purely due to DIC measurement regarding DIC algorithm parameters and test specimen surface pattern can be isolated and quantified. To numerically deform a digital image, the FEA nodal displacements are typically mapped by interpolation to deform the reference image at each and every pixel location. Pixels are displaced based on the nodal and inter-nodal displacement values. [12,17] In this work, a cubic interpolation scheme was used to determine subpixel displacements in the digital image. In addition to mapping displacements from the FEA mesh to the digital image, the predicted FEA strain field is also mapped back onto the digital image at each and every pixel location in order to compare the DIC measured strain results. Discrepancies in the comparison between measured DIC and predicted FEA strains can arise, not just due to inaccuracies associated with the DIC image tracking algorithm, but also due to errors associated with numerical interpolation. To isolate this error, an ideal speckle pattern image, generated using the Perlin noise technique [20] is also deformed using the same numerical displacement field. Differences between the measured DIC strain field created by tracking the tapestry image and that created by tracking the ideal speckle pattern, can be used to isolate the ‘tapestry image error’, *i.e.* the error specifically associated with the use of the tapestry image to track displacements since interpolation error will be the same in both images.

Focusing on the vertical component of the strain tensor distribution, the percentage difference error, PD, at each pixel location within the ROI, between the full strain field predicted by the FEA and that measured by the DIC is calculated as,

$$PD = \left(\frac{DIC_{strain} - FEA_{strain}}{FEA_{strain}}\right) \text{ x } 100 \quad (1)$$

PD is superposed onto both the tapestry and speckle images, within the ROI, producing a map of PD error distribution across all data points. This helps to visualise the full-field accuracy of the DIC measurement. The advantage of using PD as the error measure lies in its simplicity, and unambiguously provides visual representation of the DIC accuracy at data point level, although care has to be taken in interpreting the PD, when FEA strains tend towards 0, amplifying the PD. This point is particularly important when visualising strains in gravity loaded specimens when strains tend to zero at the bottom end of the hanging specimen (see Section 4.2).

2.2 DIC Settings

The DIC analysis was performed using VIC-2D (2009) software from Correlated Solutions [21]. There are many different DIC user-defined parameter setting that can influence strain measurement, including step size, subset size, strain filter size (and limits) and incremental vs non-incremental correlation; the latter usually tend to be set at default values in the DIC software but for non-ideal tracking images their optimum settings are not obvious and therefore constitute the focus of this study. To begin, the subset size and step sizes were set at 39x39 pixels and 3 pixels respectively, while the strain filter size was set at 15. The step size was kept constant for all cases examined in this investigation, while the subset size and strain filter size were later changed to 79x79 and 59x59 pixels respectively in Case 1 (see Sections 2.4.1and 4.1.2) to compare the effect of large subset size and large strain filter size on the full-field strain resolution. The aim is to evaluate the influence of subset and strain filter size on DIC performance at low strain values when using the inherent tapestry image as the target pattern. Strain is calculated using the Hencky (logarithmic) strain tensor. To ensure the most accurate DIC algorithm measurement results, the correlation criterion used is the zero normalised squared differences, using an optimized 8-tap splines interpolation shape function and Gaussian weighting for the subset weight. Other options for thresholding in the VIC-2D software are left at default values. The same DIC parameters were used for tracking both the tapestry and speckle images. The choice of zero normalised squared differences as a correlation criterion is to minimise the influence of image contrast and brightness while the choice of higher order 8-tap splines for interpolation shape function is to achieve a highly accurate sub-pixel grey level interpolation.

2.3 Description of Tapestries

Images of two historic tapestries and a fragment from another historic tapestry are used to evaluate DIC measurement accuracy. The tapestries are shown in Fig. 1 '*The Acts of the Apostles: St Peter Healing the Lame Man*' [5] (Tapestry 1), Fig. 2, '*The Story of Esther*' (Tapestry 2) [5] and Fig. 3, a fragment from a larger un-named tapestry from the Karen Finch reference collection (Tapestry 3). Assumed dimensions and areal densities used in the numerical simulations are provided in Table 1. Tapestries 1 & 2 are chosen because of their different features: Tapestry 1 includes broad regions of uniform colour, with little information

for DIC algorithms to track. In contrast, Tapestry 2 is a more random and intricate image, containing high contrast patterns. Tapestry 3 is chosen because of its poor physical condition; it contains several open slits (tears) and other areas of damage and is included to demonstrate the potential use of DIC in assisting conservators understand the influence of damage and conservation measures, such as slit patching, on the tapestry's structural integrity. The true coloured (RGB) images are first converted to greyscale images suitable for DIC analysis, using the MATLAB [22] rgb2gray function. To illustrate the relative size between subsets and tapestry image detail used in this study, a greyscale image of Tapestry 1 with two subset sizes mapped over the image is shown in Fig. 4. The grey scale intensity distribution of each image is also plotted as a histogram in Fig. 5. Comparing the greyscale intensity distribution of the tapestry images against that of an ideal speckle pattern (which has a random grey intensity distribution), highlights the differences. The grey scale intensity distribution plot reflects the distinct features and distribution of random patterns on the tapestry images, ideally this would follow a Gaussian distribution. Of the three tapestry images, Tapestry 2 has the most ideal distribution. It is emphasised here that the present study is wholly based on numerical simulations and therefore no hardware setup required. Only the initial reference/undeformed image of Tapestry 3 was acquired by the authors, using a Canon EOS 1000D™ (manual mode, no flash, 100 ISO, f/8 aperture, exposure time 1/4 s). Camera settings and hardware setup details for Tapestry 1 and 2 images are not known.

2.4 Description of Case Studies

The goals of the following case studies are to demonstrate: (a) how the technique of synthetic image deformation can be used to provide insights into determining the optimum DIC parameters settings and (b) how the method can be used to manage expectations for both full-field and globally averaged DIC measurement accuracy on historic tapestries.

2.4.1 Case 1 using Tapestry 1: Displacement Controlled Deformation at Low Strain Levels

In the first case study, a similar sensitivity analysis using Tapestry 1 to that provided in Alsayednoor et al. [17] is demonstrated, though here the importance of various other parameters on DIC accuracy is explored. In particular:

a) while Alsayednoor et al. [17] examined the accuracy of DIC at strains of up to 7% under self-weight load, here much lower strains of just 1% are considered; a more realistic and challenging strain measurement scenario. The challenge is that at such low strain levels, the signal to noise ratio for DIC measurement on a heterogenous tapestry structure containing a complex strain field, could be very low.
b) the effect of incremental vs non-incremental strain measurement is examined,
c) the influence of the strain filter size is examined.

The use of a relative full-field percentage difference error map (see Section 2.1.2) is introduced to give a more quantitative estimate of local errors. The fixed constraint in this study is the tapestry image itself. By comparing the results obtained by tracking the tapestry image with those produced using the speckle pattern, the user can better understand the reduction in accuracy attributable to the use of a non-ideal target image. For this analysis, a known displacement magnitude (1% of the image height) is applied to the bottom of the FE tapestry model to generate a heterogeneous deformation in 5 equal displacement increments, producing five digital images with gradually increasing deformation.

2.4.2 Case 2 using Tapestry 2: Self Weight Loading

The second case study is used to investigate the influence of image resolution on DIC performance, using the inherent tapestry image to track displacements when the tapestry is loaded under its own self weight. The self-weight load is applied using the Abaqus [23] gravity body force load function, making use of the assumed areal density of Tapestry 2 (see Table 1). The image resolution was varied using the Matlab image resize function [22], and the error associated with changes in the image resolution is quantified. The latter helps the user understand the influence of image resolution on the DIC measurement and provides a means of optimising the camera resolution prior to performing the actual DIC tests.

2.4.3 Case 3 using Tapestry 3: Time dependent loading due to changing humidity

Previous researchers have noted a strong correlation between the globally averaged strain measured using DIC, and environmental relative humidity levels [10,24]. In Costantini et al. [24] long term DIC monitoring (200 hours) of Tapestry 3 was conducted while simultaneously recording the environmental relative humidity; a correlation coefficient of 0.92 was found between the DIC measured globally averaged strain and the relative humidity variation. The results showed that the globally averaged strain measured by the DIC closely follows the measured relative humidity change. The aim of that investigation was to better understand potential damage mechanisms occurring in displayed tapestries. Detailed description of the test conditions and DIC measurement setup can be found in Costantini et al. [24] This strong correlation demonstrated that the globally averaged strains within the ROI were certainly measuring strains related to environmental humidity and effectively demonstrated the validity of the globally averaged DIC measurements. However, the question of whether achieving accurate globally averaged DIC strain measurements necessarily implies that local DIC strain measurements are also accurate, remained unanswered. This is a relevant and important question when aiming to understand the influence of localised cyclic strains on the subsequent localised tapestry damage. Consequently, in this third case study, a numerical model of Tapestry 3 was subject to a time varying load to generate globally averaged tapestry strains of similar magnitude to those induced by fluctuations in relative humidity. To do this, the gravitational load on the Tapestry 3 model was varied using values designed to mimic the actual strains induced by the time-humidity variation. [24].

3. Numerical Simulations

The finite element models used to create representative synthetic deformations in this study are meshed with four node rectangular membrane elements (M3D4R) in the FEA software, Abaqus [23] (see Fig. 6a for example mesh). Two areas have been identified in the images using the Canny edge detection algorithm and are representative of the different cloth and stitching zones as described in the Section 2. Each zone is assigned different material properties (see Section 3.4) in order to generate a representative heterogeneous deformation field. The digitally generated image with ideal speckle pattern (section 2.1.2) is shown in Fig. 6b.

3.1 Model Size

A convenient method to accurately map displacements and strains involves scaling the outer dimensions of the tapestry image (measured in pixel units) and FEA simulation (measured in length units, such as mm) to have the same number of units. This approach means that tapestry

images obtained from tapestries of unknown physical dimensions can be easily analysed. Two methods can be used to achieve this. A common approach is to use the digital image dimensions and match the FE model dimensions accordingly [8]. For example, a 1000x2000 pixel image might be used to create a 1000x2000mm sized 2D finite element model of the tapestry, even if the tapestry size is significantly different to this. If the user then wants to correctly predict stresses in the tapestry (e.g. if damage is to be modelled), then the material's mechanical behaviour is required and if the model is loaded under its gravitational self-weight, the material density has to be scaled according to the ratio between the actual tapestry size and the FEA model size. If on the other hand, the main purpose of the exercise is simply to evaluate the accuracy of DIC strain measurements, and the user is not interested in stresses, then a displacement boundary condition can be imposed in the FEA model (e.g. a 1 mm downward displacement of the bottom edge), in this case, material mechanical properties and density scaling are not important. The second approach matches the FEA model size to the actual tapestry size and to then resizes the tapestry image accordingly. Actual material properties can then be used to predict the stresses/strains under self-weight loading with no need to scale the material density. However, resizing the reference image can affect the image resolution and can potentially influence the accuracy of the subsequent DIC measurements. A goal of this investigation is to investigate the influence of resizing the reference image on the accuracy of the DIC measurements.

3.2 Relative Mesh Density

As mentioned in the previous section, the FEA model and tapestry digital image are of the same numerical outer dimensions in length scale. However, the required number of nodes (by extension, the number of elements) in the FEA model to achieve a refined spatial resolution of the deformation field is usually much less than the number of pixels in the digital image. To reduce computational cost and also achieve optimum mapping of the deformation field generated by the FEA model onto the tapestry image through interpolation, a 'relative mesh density value' is used. The relative mesh density is the ratio of the number of pixels in the digital image to the number of finite elements in an FE model per unit side length and determines the number of pixels in a finite element. Selection of the relative mesh density determines the FEA mesh density (fine or coarse discretization) relative to the number of pixels in the digital image. For example, a relative mesh density value of 1 means 1 pixel to 1 element. In all the FEA analysis, mesh density value of 5 was used, producing mesh independent deformation fields used in the numerical image deformation and strain fields for DIC error measure.

3.3 Loading and Boundary Conditions

In all cases, the upper side of the tapestry model is fixed using an encastre boundary condition to replicate the hanging condition used in museums and historic houses. Loading was applied in two ways: (a) by a known displacement magnitude applied at the bottom of the tapestry and (b) by the tapestry's self-weight loading due to gravity.

3.4 Material properties used in Simulations

When loading the tapestry model using self-weight, characterisation of the fabric's mechanical properties and density are essential if a reasonably representative deformation field is to be predicted using FEA. To this end, Alsayednoor et al. [17] used a nonlinear hyper-elastic Ogden model. [25] fitted to experimental data. However, if an imposed displacement along the bottom

edge of the tapestry is used to generate strains in the FEA, and the user is not interested in predicting stresses, then the actual material stiffnesses and densities are not so important. More significant in determining the heterogenous strain field is the relative stiffness of the two materials, cloth and stitching, within the tapestry. Use of an imposed displacement assumes that the user has a good idea of the size of strains one might expect to observe when loading a tapestry under self-weight. Also, for the purpose of error assessment and sensitivity studies, such as investigations into the influence of tapestry image resolution on DIC performance, use of accurate material behaviour is not critical. As such, for simplicity, all Case Studies use linear elastic behaviour with a Young's modulus and Poisson's values of 120 MPa and 0.4 respectively for the tapestry cloth a lower Young's modulus value of 60 MPa for the stitching. This results in the prediction of a complex heterogenous strain field, even when applying a constant displacement along the bottom edge of the tapestry. This heterogeneous displacement field is used to deform both the tapestry and the ideal speckle pattern images. The thickness of the tapestries is assumed to be 1mm.

4. Results and Discussion

The vertical component of the logarithmic (also known as Hencky/true strain) strain tensor represented as e_{yy} in VIC 2D or LE22 in Abaqus is used for the analysis and discussions in the following sections. This is because the vertical component of the strain tensor is more significant than other strain components due the loading conditions applied. The Hencky strain tensor is an incremental strain measure suitable for both small and large deformations. The general expression for Hencky strain tensor is obtained by integrating the incremental strain over the load steps giving;

$$\varepsilon = \ln\left(\frac{l}{L}\right) \tag{2}$$

where L is the initial length and l is the final length.

4.1 Case 1: Displacement Controlled Deformation on Tapestry 1

The displacement field from the FEA predictions and DIC measurements (filter size = 15 data points, and a subset size = 39x39 pixels) are shown in Fig. 7 at both the first (0.2% imposed average strain) and last (1% imposed average strain) load step. Note these initial DIC settings used have yet to be optimised; they are simply an initial reasonable guess, motivated by the anticipated trade-off between achieving an acceptable resolution when measuring a heterogeneous strain field, and accuracy. Results are given in pixels and the negative value implies a downward displacement. As expected, the displacement field obtained from the FEA simulation scales linearly with load (compare Figs. 7a and 7d). The measured DIC displacement field produced when using the speckle image to track displacements, closely follows that of the FEA simulation at both 0.2% and 1% imposed average strain (compare Figs. 7a and 7c and Figs. 7d with 7f). In contrast, the DIC-measured displacement field, produced when using the tapestry image to track displacements, shows notable discrepancy with the FEA simulation at 0.2% imposed average strain (compare Figs. 7a and 7b) but performs better at 1% imposed average strain (compare Figs. 7d and7e). The corresponding displacement percent error maps from the tapestry and speckle images at the two load steps are shown in the Fig. 8 (see Equation 1). As expected, error decreases with strain magnitude for both tracking images

(speckle and tapestry), though the speckle image produces a notably more accurate DIC displacement measurement than the tapestry image at low average strains of 0.2%. As might be expected, DIC measurement errors of displacement are high at locations with low tracking information (the relatively isotropic regions shown in Fig. 1).

Fig. 9a shows the FEA-predicted strain field (in the vertical direction e_{yy}) mapped onto Tapestry 1 at the final load step of 1% imposed average strain. The mechanical heterogeneity of the tapestry clearly creates localised strains that are both higher and lower than the globally imposed average strain of 1%. Once again, a strain filter size of 15 points and a subset size of 39x39 pixels were used. Figs. 9b and 9c shows that the fine details of the FEA strain predictions are lost in the DIC measurements using both the tapestry and speckle images to track strains and 'error waves' appear, orientated in the horizontal direction. This error is not so apparent in the displacement field measurements (Fig. 7) and is introduced when calculating strains, which is a known source of extra error in DIC measurements [26]. The error waves are due to the low signal to noise ratio and, when using these particular DIC settings, demonstrate an inability of the DIC technique to measure the intricate strain field produced in the Tapestry image at low strain levels when using the tapestry image to track displacements. To better understand the influence of a low signal to noise ratio on DIC strain measurements, a homogeneous strain field (produced using homogenous material behaviour) is shown in the Fig. 10. The high strain values at the top corners of the FEA reference strain field are due to the Poisson's effect and can be ignored. Comparing Figs. 9a and 10a shows the difference between the homogeneous and the more complex heterogeneous strain fields. The DIC measurements produced using both the tapestry image (Fig. 10b) and the speckle pattern (Fig. 10c) both contain error waves. Although the results are not presented in the current study, applying low pass filter in the DIC calculation reduced the error waves with speckle image (only for homogenous material assumption with some "error waves" still present) but produced no improvement with tapestry image. Low pass filter reduces aliasing effects (aliasing is an effect that causes different signals to become indistinguishable when sampled) by removing some high-frequency information from images. The influence of low pass filtering on DIC measurement accuracy using tapestry inherent surface pattern at low strain levels is the intended future work.

The strain fields from a higher strain level with 10% imposed strain is shown in the Fig. 11 for both homogenous and heterogenous strain fields. Using the same DIC settings, the DIC accuracy improved significantly, the "error waves" are eliminated, showing that signal to noise ratio affects DIC accuracy more than strain field complexity. These results show that, for given DIC settings, there is a dependence between strain level, specimen tracking pattern and the strain field complexity, on DIC accuracy.

Some of the rough details of the FEA strain prediction are reproduced in all results (Fig. 9), though additional and erroneous areas of high strain are also apparent in the DIC measurements, especially when using the tapestry image to track strains. In practice, when using these DIC settings, the user would be unable to distinguish real and erroneous regions of high strain with certainty, instead the DIC results can only suggest 'probable' regions of high strain. As expected, DIC tracking using the speckle image (Fig. 9b) produces more accurate strain measurements, i.e. closer to the FEA prediction, than measurements made using the tapestry image (Figs. 9c and 9d).

4.1.1 Influence of Incremental Correlation

The DIC option of 'incremental correlation' is found to increase error when using the tapestry image to track deformations (compare Fig. 9c & Fig. 9d) though has relatively minor influence when using the speckle pattern, as will be evidenced when examining the average global errors.

Fig. 12(a-d) shows the strain field percentage error maps (see Equation 1) after applying a final load step of 1% imposed average strain. The full-field error maps are produced by comparing the strain measurements from the DIC algorithm after tracking the deformations using both the speckle pattern (Fig. 12a and Fig. 12c) and the tapestry image (Fig. 12b and 12d) using both incremental and non-incremental correlation (see Table 2 for definition). In all percentage error maps in this investigation, the limits displayed by the colour scale is 0 to 55%, higher values are shown in grey, negative values are shown in black. The range is chosen to help compare details in the various error maps. Figs. 12b and 12d show that locations with higher percentage error (above 55% error) are more common when using the tapestry image. The highest errors in the error maps correspond to locations in the tapestry image with fewer trackable features (low information density), referred to as isotropic regions in Fig. 1. As mentioned for Fig. 9., use of 'incremental correlation' is found to increase error when using the tapestry image to track displacements (compare Fig. 12b and Fig. 12d). The increased error from incremental correlation is assumed to be due to error propagation. Hence, incremental correlation should not be relied upon to improve DIC measurement accuracy when using only the tapestry natural surface pattern for deformation tracking. This is in contrast to the observations in [17] where incremental correlation was reported to improve DIC accuracy using tapestry's natural surface pattern for tracking deformation. Although, the study in [17] is at a much higher strain level.

The strain field percentage error maps produced when analysing the: (i) homogeneous strain field at 1% imposed average strain, (ii) the heterogeneous strain field at 10% average imposed strain and (iii) the homogeneous strain field at 10% imposed average strain, are all shown together in Fig. 13. The percent error is lower for the homogenous strain field measurements when compared with heterogenous strain field measurements at low average-imposed strain (1%). This supports the observation that strain field complexity in addition to signal to noise ratio affects DIC accuracy severely. At higher strain levels, the percent error reduces to less than 2% when using the speckle image while higher error values are seen around the isotropic regions when using the tapestry image to track displacements.

Plotting the average global percentage error within the ROI (see Section 2.1.1 for definition) versus the average global strain as the simulation progresses reveals information on the relative global accuracy of the various methods of tracking displacements, when using these specific DIC settings (see Fig. 14). The average global percentage error is calculated in the same manner as the average global strain within a ROI. That is, the global average percent error in any given ROI is calculated simply by calculating the sum of the percent error across all pixels in a given ROI, divided by the number of pixels. As expected, Fig. 14 shows that using a speckle image to track strains results in lower globally averaged error than when using the tapestry image. Use of incremental tracking has little influence when using the speckle image but reduces the accuracy when using the tapestry image. Also notable in all the data in Fig. 14 is the clear decrease in the globally averaged error with increasing global strain, i.e. the DIC method becomes more reliable as the average imposed strain level increases.

4.1.2 Influence of Strain Filter and Subset Size

As mentioned earlier, the DIC settings used in Section 4.1.1 were simply an initial reasonable guess and were not in any way 'optimised'. The process of iteratively comparing DIC measurements with known synthetic FEA-generated deformation fields when using different DIC settings does allow for some degree of optimisation. For example, Alsayednoor et al [17] found that increasing the subset size improved accuracy at the cost of reducing resolution in the measured full-field strain image. In this investigation we demonstrate the effect of other DIC parameter settings and examine the influence of the strain filter size (used to calculate the strain field from the displacement field) and compare the effect of using a large strain filter size to that found when using a large subset size, on strain field resolution and error measurement. Non-incremental correlation is used for both cases.

First, a large strain filter size value of 59 was used (increased from the value of 15, used in the previous section), while keeping the subset size at 39x39 pixels. The strain fields for the tapestry and speckle images are shown in Fig. 15a and 15b, while the global average percentage error versus the global average strain plots are shown in Fig. 15c. Fig. 15a and 15b show that the resolution of the measured strain field is reduced by increasing the strain filter size, in this case 'blurring' many details within the results. The larger data points used in calculating strain smooth out the heterogeneity in the strain field. Results produced using the speckle pattern and tapestry image converge and the 'error waves' apparent in Fig. 9 are eliminated. The overall measurement accuracy is significantly improved as indicated by the global average percentage error, shown in Fig. 15c (compare with Fig. 12). Thus, the use of a larger strain filter size can help the user decide which of the high strain regions are valid when examining results calculated using smaller filter sizes.

The next example uses a 79x79 subset size and reverts to a strain filter size of 15 points (as used in Section 4.1.1). By comparing the results obtained with a large strain filter size combined with small subset size (Fig. 15) and large subset size combined with small strain filter size (Fig. 16), it is evident that the intricate and distinct strain pattern obtained from the FEA results (see Fig. 9a) are better replicated in the second case (Fig. 16) than the "blurred" strain produced in the first case (Fig. 15). A large strain filter size combined with a small subset size produces a lower global percent error with low strain resolution while large subset size combined with a small strain filter size produces a higher strain field resolution but higher global percent error. The analysis from the first and second examples has shown that there is a trade-off between achieving high strain resolution and low global percent error using the tapestry natural surface for DIC measurement. If high full-field strain resolution is desired with minimal computation cost, a large subset size (in this study 79x 79 pixels) should be used and combined with a small filter size (15 in this investigation). However, if low global percent error is required, a large strain filter size should be used in the DIC analysis.

4.2 Case 2: Self-Weight Loading using Tapestry 2

The finite element model dimensions for the analyses presented in this section were determined using the second approach described in the Section 3.1, i.e. the model size (in mm) was set equal to the actual size of the tapestry and the tapestry digital image resized using scale factor of 1:1 (i.e., 1 mm in the FEA dimension is equivalent to 1 pixel in the digital image). Changing the image size means that the image resolution will change. Note that the number and size of

elements in the finite element mesh is decided by the user and is independent of the dimensions of the outer perimeter of the FE model.

4.2.1 Influence of Image Resolution

Understanding the influence of image quality (in terms of resolution) on DIC measurement accuracy is important because it helps the conservation scientist to determine how the image resolution (due to camera settings and noise, lens distortion, camera misalignment, blurring and contrast) might affect the subsequent DIC measurements, especially when the latter uses the tapestry image to track displacements. This is because DIC measurement accuracy depends fundamentally on the identifiability of distinct and random tracking features on the tapestry's surface. The identification of these distinct features for DIC matching can be enhanced/impeded with image resolution; hence image resolution affects DIC accuracy. The effect of image resolution is examined under the self-weight loading condition (see Section 2.4.2) using images of Tapestry 2 at different resolutions. To do this, image resolution/quality was varied using the MATLAB image resize function (*imresize*). The original digital image is resized by the required resolution reduction factor and then, again using the image resize function to change the reduced image size to the original image dimensions in pixels. The tapestry image resolution was reduced by 2 (i.e. reduction factor is 0.5) and then by 5 (i.e. reduction factor is 0.2). The results of the DIC analysis (again employing a 15 data points strain filter size with 39x39 pixels subset size and mesh density value of 5) using digital images with reduced resolution are shown in Fig.17. The strain fields from FEA, DIC measured strain field using Tapestry 2 and speckle pattern original images (i.e. without reduced resolutions) using the same DIC parameters are all shown in Fig 18. The plots in Fig. 18 are to be compared with strain fields in Fig. 17. It should be noted that the FEA strain field is the same for all image resolutions. The results in Fig. 17 show that, as expected, the DIC measurement accuracy decreases with image resolution and that the influence of image resolution on the DIC measurement is much more severe when using the tapestry image instead of the speckle image. This observation becomes evident by comparing the strain resolution obtained from the original image in Fig. 18 (b and c) and strain fields obtained from the reduced image resolution in the Fig. 17. Also, the percent error map obtained with the low resolution (see Figs. 19a to 19d) and the percent error map obtained with the original image (see Figs. 19e and 19f) showed that the low-resolution image produced higher error regions. Overall, the loss of DIC accuracy with reduction in image resolution can be attributed to the loss of both contrast variation in the images and matching quality of DIC algorithm as the intrinsic patterns on the tapestry surface become blurred and unidentifiable appearing "smoothed". The loss of DIC measurement accuracy due to poor image resolution can be compensated by increasing the subset size but at the cost of spatial resolution. The analysis demonstrated how the method developed in this study can be used to pre-analyse a given tapestry image prior to conducting experiments. The tool potentially enables tapestry conservation scientists to ascertain the influence of image obtained from available camera hardware on DIC accuracy and determine the trade-off between image quality and strain resolution when choosing the DIC parameters.

4.3 Case 3: Time dependent loading due to changing humidity using Tapestry 3

The aim of this case study is to recreate similar fluctuating strains to those measured by Costantini et al. [24] that occur in response to changing environmental relative humidity. To do this numerically, a model of the tapestry fragment was loaded under time varying self-weight, the size of the load was varied by changing the areal density over time (see Fig. 20). The changing self-weight of the model was adjusted to recreate similar time varying strains to those measured by Costantini et al. [24] These numerical strains were then analysed using DIC to evaluate the effectiveness of DIC in measuring both globally averaged (also included in Fig. 21) and full-field strains (see Fig. 22).

The predicted FEA strain field and the DIC measured strain field for the last time instant at approximately 0.07% global average strain level is shown in Fig. 22a and 22b respectively while the Fig. 22c and 22d show the strain field at a higher strain level of 0.1% at time 100 hours. The Fig. 22 again highlighted the accuracy dependence of DIC measurement on strain levels. The results of the experimentally measured strain field occurring across Tapestry 3 at the last time instant can be found in [24]. Four tears referred as slits in [24] (simulated as deleted elements in Abaqus) have been included in the FE model at similar locations to those observed in Tapestry 3 (see Fig. 22). The local strain fields in Fig. 22 are similar overall especially at higher strain levels, except near the crack tips, where highly localised high strains are visible in the FE predictions, showing the usual "dog bone" shape associated with crack tips. In contrast, the DIC measurements show large positive strain values across the tears/cracks, referred to as pseudo strain which are not real strain fields but from DIC inherent error. [17, 24] This is because the low resolution in the DIC measurements leads to interpolation of displacement across the opening tear, which is interpreted as a large positive strain. These pseudo strains could be misinterpreted as true large strain and could cause lack of trust in the DIC measurement results. These tears can be masked or cut-off during the DIC computation setup. However, this is not recommended because the crack tip can be removed which means that strain/stress field around the crack tips/strain intensity factor could be screened out, masking essential details which could assist in determining the extent of required areas for patching/slit stitching. Because crack areas are very small compared to the overall tapestry dimensions, these high strain values do not significantly affect the global averaged strain values. Therefore, if the aim of such analysis is to use global average strain values from DIC for analysis, then masking tears is not necessary.

The results of the analysis have been used to match the global strain variation with RH fluctuation. By comparing the global average strain plots against time in the numerical analysis and the actual test (Fig. 21), it can be seen that the predicted strain trends are similar with the average global strain values measured experimentally. Analysis of the global average error shown in Fig. 23 showed that the percent error is higher at lower strain values than at higher strain values which is consistent with the overall observation from this study.

This case study has replicated the experimental tests conducted in [24] and showed that indeed global average strain variation due to slight changes in the tapestry display environment can be adequately captured by DIC measurements. In this analysis, the material properties have been assumed to be elastic, nonetheless, nonlinear material properties such as hyperelasticity predicted similar trends as well [17]. The close correlation between plots in Fig. 21 and Fig. 22 with experimental results published in [24] suggest that the systematic approach developed in

this investigation can be used to validate complex DIC analysis such as fatigue and creep damage mechanics of tapestry due to the humidity and temperature variation.

5 Conclusions

It has been shown that the accuracy of the DIC measurement is load/deformation level dependent and care should be taken when using tapestry inherent features as tracking information in DIC analysis. The analyses at low strain level showed that using small subset size and strain filter values which ideally should produce higher resolution of the DIC measured strain field increases background noise especially when using tapestry inherent surface pattern for DIC deformation tracking. Alternatively, using large strain filter size and subset size values reduces background noise but hides intricate strain details. Therefore, a trade-off has to be struck. The optimum DIC settings depend on (strain field magnitude/heterogeneity/tracking image) and the only way to determine them is by a parametric study using synthetic deformation fields to guide the optimisation process, i.e. using a tool such as the one developed in this study. For optimum DIC performance using inherent tapestry, it is recommended that:

1. use of incremental correlation in the DIC analysis is avoided, due to accumulation of error. Although with high quality speckle images or high strain values (>7%), incremental correlation has been recommended to improve DIC measurements, it is also a well-known fact that noise accumulation is exacerbated by small errors in the displacement measurement and this error is amplified in the strain results. To avoid additional error in strain measurement using DIC techniques due to accumulation of noise, incremental correlation should be avoided.

2. a relatively large subset size values is used, such as 79x79 pixels under low load strain levels to reduce noise in the strain results. Because the size of features on a typical tapestry is arbitrary, generally of low contrast, highly heterogeneous and cannot be anticipated, there is no one-size-fits-all method to suggest optimum subset size selection for tapestry images. An arbitrarily chosen large subset size could result in the loss of spatial distribution of the strain field and over smoothing. Using large strain filter values also could result in over smoothing of the strain field and masking of potential strain concentration zones. Consequently, the size of the optimum subset size and strain filter size for a given tapestry should be determined iteratively ideally by making use of the kind of synthetic deformation fields employed in this study, prior to conducting actual DIC tests.

3. a high-quality digital image of the tapestry should be used in the DIC analysis. This can be achieved by using a suitable imaging system (camera system resolution and high-quality camera lens) and appropriate lighting conditions during the DIC experiments to reduce image noise. The influence of the imaging system and the lighting conditions can be evaluated prior to experiments, using the approach and techniques developed in this study. In that case, the code developed for this study is published on GitHub [27] and can freely be used for similar investigations. Also, the analysis from artificially varying the Tapestry 3 areal density which mimics changes in the humidity showed that small variations in strain levels can reliably be captured by DIC measurements. This

ensures that delicate tapestries can be continuously monitored using DIC measurement system.

While these conclusions are based on the effects of DIC parameter setting and image resolution, as outlined in this investigation, it should be noted that other random and systematic sources of error in the DIC measurement, such as out of plane displacement, non-planar measurement surfaces and issues originating from test setup such as noise associated with image acquisition, can significantly affect the measurement results. This makes error quantification in the DIC measurement chain non-trivial. Nevertheless, most of these errors, which are often related to the test setup, have potential solutions. For instance, while out-of-plane displacement of the test surface is sometimes unavoidable, this problem can be mitigated using 3D DIC analysis (a two-camera stereoscopic system) or by conducting 2D DIC but with increased distance between the test surface and imaging system, to produce a telecentric effect. Lens distortion can be compensated for by using better correlation algorithms and/or adequate calibration during tests. Image noise due to changes in lighting conditions can be reduced by selecting appropriate correlation algorithms and through the use of a high-performance imaging system that can reduce the noise inherent in image acquisition hardware. Clearly, due diligence is required to minimise systematic sources of error, however, using the approach outlined in this study, uncertainties associated with DIC algorithm parameter settings and image quality can be examined in order to evaluate the suitability of a given inherent tapestry image for use as a DIC tracking pattern, and to help distinguish between true measurement strains and noise.

Acknowledgements

The authors are thankful to the Leverhulme Trust for the grant (Ref: RGP-2015-179), “From the Golden Age to the Digital Age: Modelling and Monitoring Historic Tapestries” through which this study was conducted.

References

1. M.A. Sutton, J.J. Orteu, H.Schreier, *Image Correlation for Shape, Motion and Deformation Meaurements. Basic Concepts, Theory and Applications,* Springer, **2009**.
2. D. Dureisseix, J. Colmars, A. Baldit, F. Morestin, H. Maigre, Int. J. Solids Struct. **2011**, 48, 1024
3. J.-C. Dupre, D. Jullien, L. Uzielli, F. Hesser, L. Rparbelli, C. Gauvin, P. Mazzanti, J. Gril, G. Tournillon, D. Amoroso, H. Massieux, P. Stepanoff, M. Bousvatou, J. Cultural Heritage, **2020** 46, 165.
4. C. Gauvin, A.K. Beall, S. Ekelund, I. Breebaart, R.K. Gotink, J.-C. Dupre, F. Hesser, P. Van Duin, and P. Noble, *ICOM-CC Conference, Copenhagen,* **2017**.
5. F. Lennard, M. Hayward (Eds), Tapestry Conservation: Principles and Practice. Series: Series in Conservation and Museology,Butterworth-Heinemann, Oxford. ISBN **2006**. ISBN:9780750661843.
6. J.M. Dulieu-Barton, L. Dokos, D. Eastop, F. Lennard, A.R Chambers, M. Sahin, *Reviews in Conservation* **2005**, 6, 63.

7. H.R. Williams, F. Lennard, D. Eastop, J.M. Dulieu-Barton, A.R. Chambers, Proc. AIC Textile Specialty Group, Loa Angeles, USA, **2009**.
8. D. Khennouf, J. M. Dulieu-Barton, A. R. Chambers, F. J. Lennard, D. D. Eastop, Strain **2010**, 46, 19.
9. F. Lennard, D. Eastop, C.C. Ye, J.M. Dulieu-Barton, A.R. Chambers, D. Kennouf, *ICOM Comnnittee for Conversation*, **2008**.
10. J.M. Dulieu-Barton, D. Kennouf, A.R. Chambers, F.J. Lennard, D.D. Eastop, *In proc. SEM Annual Conference*, **2010**, Indianapolis, US.
11. D. Lecompte, A. Smiths, S. Bossuyt, H. Sol, J. Vantomme, D. Van Hemelrijck, A.M. Habraken, Opt. Lasers Eng. **2005**, 44, 1132.
12. Y. Wang, P. Lava, S. Coppieters, M. De Strycker, P. Van Houtte, D. Debruyne, Strain **2012**, 48, 453
13. P. Lava, S. Cooreman, S. Coppieters, M. De Strycker, D. Debruyne, Opt. Lasers Eng. **2009**, 47, 747.
14. P. Lava, S. Cooreman, D. Debruyne, Opt. Lasers Eng. **2010**, 48, 457.
15. T. Hua, H. Xie, S. Wang, Z. Hu, P. Chen, Q. Zhang, Opt. Laser Tech. **2011**,43,9.
16. Y. Su, Q. Zhang, X. Xu, Z. Gao, Opt. Lasers Eng. **2016**, 86,132.
17. J. Alsayendoor, P. Harrison, M. Dobbie, R. Constantini, F. Lennard, Strain **2019**, 55,1.
18. VIC 3D Manual, Online Documentation n.d.
19. H. Pan, Z. Guo, T. Hua. Opt. Eng. **2007**, 3,1.
20. J. J. Orteu, D. Garcia, L. Robert, F. Bugarin, From Grains to Flowers **2006**, 6341, U110.
21. VIC-2D is a product of Correlated Solutions Inc., https://www.correlatedsolutions.com/
22. Matlab, MathWorks®, Online Documentation n.d.
23. Abaqus, *ABAQUS* is a product of ABAQUS Inc, www.3ds.com
24. R. Constantini, F. Lennard, P. Harrison, J. Alsayednoor, J. Euro. Phy. **2020**, 125.
25. R.W. Ogden, Chem, Tech. **1973**; 46,398.
26. B. Pan, K. Qian, H. Xie, A. Asundi, Meas. Sci. Techno. **2009**, 20, 062001.
27. https://github.com/PhilipHarrisonGlasgowUni/SynDIC

Fig. 1. The Acts of the Apostles: St Peter Healing the Lame Man [5]. The white boxes show typical isotropic regions prevalent in the image while the blue box shows typical large dark regions also present at different locations in the image.

Fig. 2. The story of Esther: Esther hearing of Haman's plot [5].

Fig. 3. A historic fragment from Karen Finch Reference Collection at the Centre for Textile Conservation and Technical Art History, University of Glasgow.

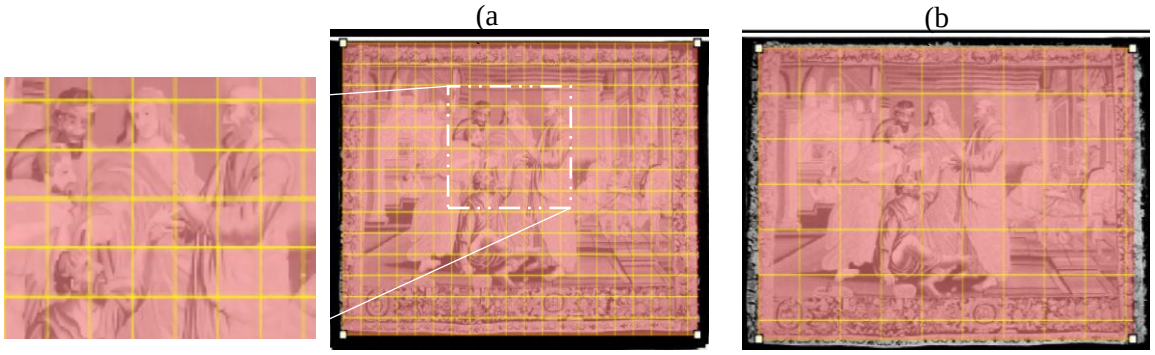

Fig.4. Greyscale image of Tapestry 1 showing the subsets sizes. (a) 39 x39 subsets. (b) 79 x79 subsets.

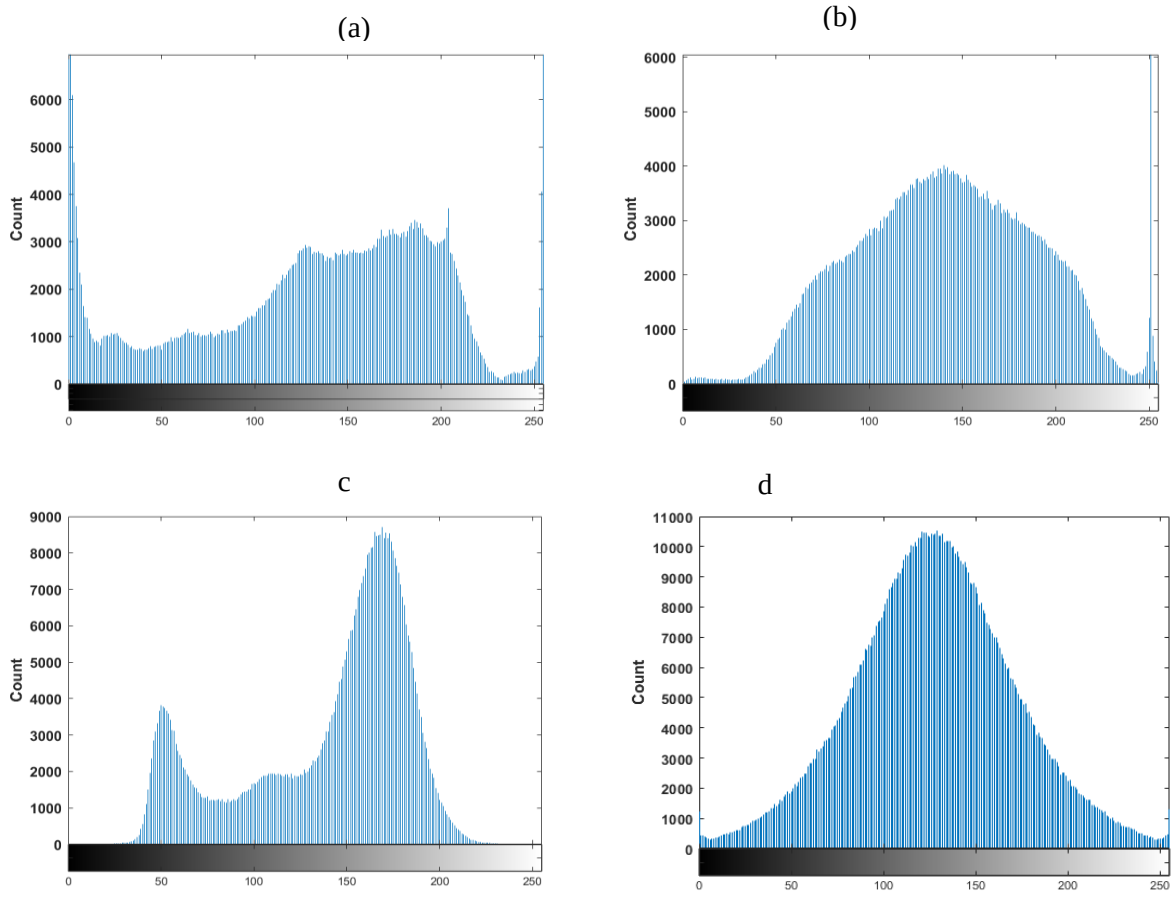

Fig.5. Grey levels distribution: (a) Tapestry 1, (b) Tapestry 2, (c) Tapestry 3 and (d) a typical ideal speckle image (see Fig. 6b).

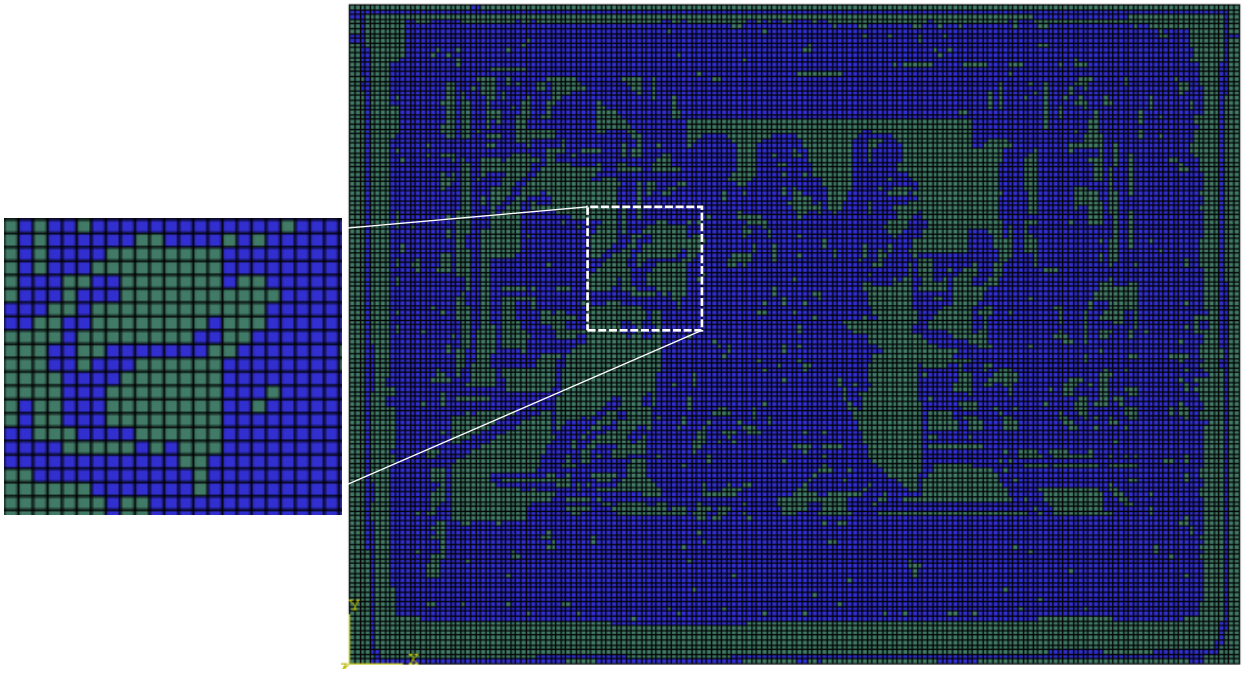

Fig. 6a. Abaqus finite element model mesh showing the distinct sections (blue colour represents stitching; the green colour represents cloth) detected using Canny Edge Detection algorithm.

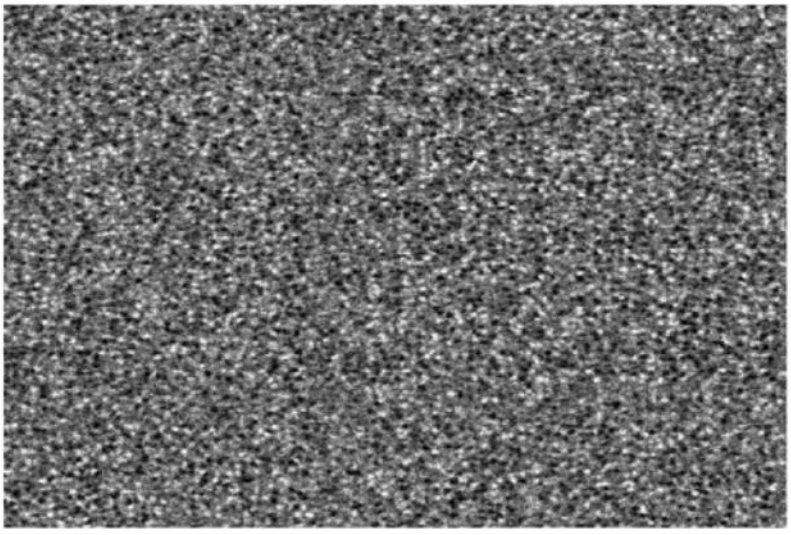

Fig. 6b. Speckle pattern image digitally generated using Perlin noise technique

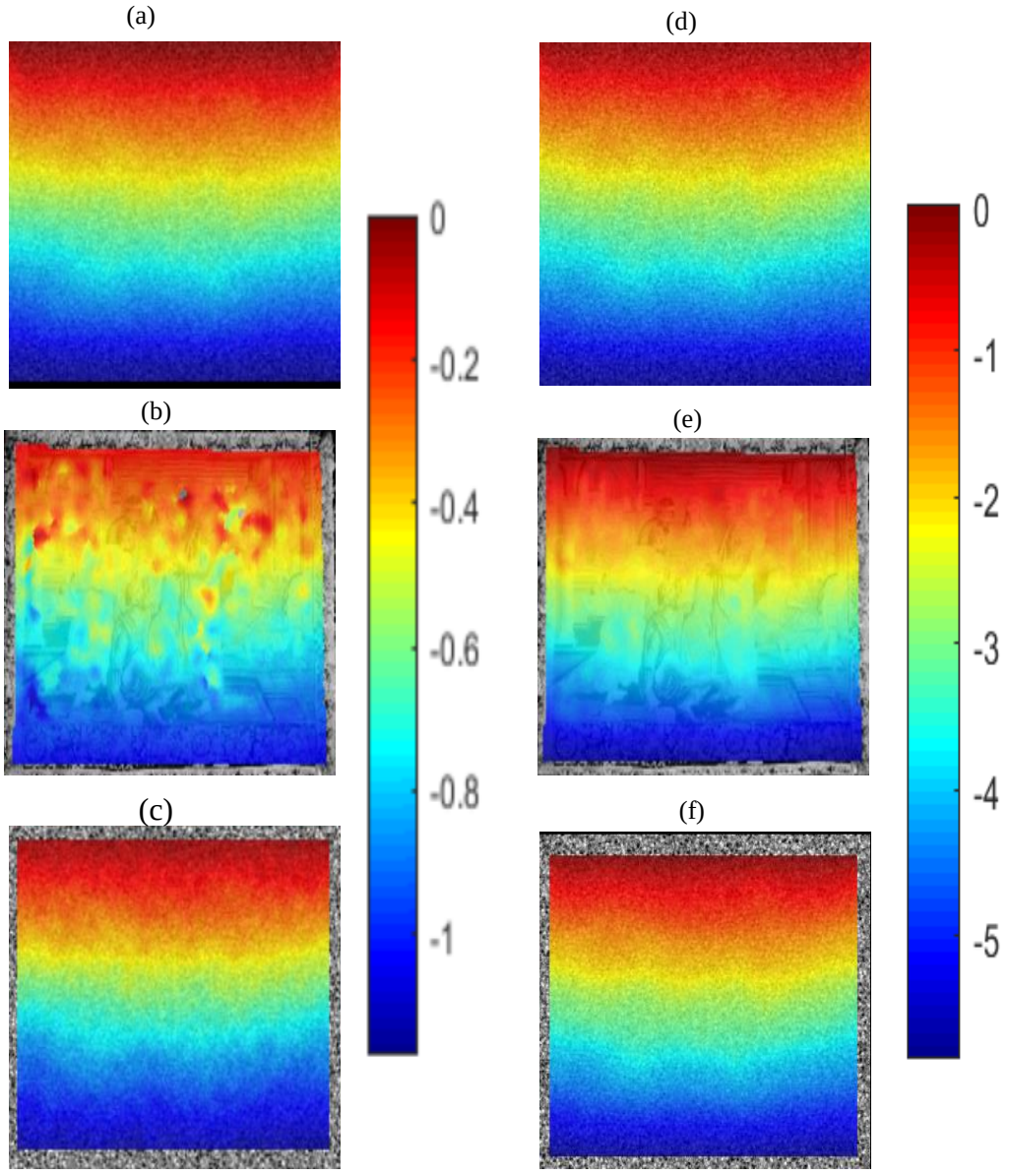

Fig.7. Displacement field in pixels. At first load step (20% of imposed displacement): (a) reference FEA, (b) DIC with tapestry and (c) DIC with speckle image). At last load step: (d) reference FEA, (e) DIC with tapestry and (f) DIC with speckle image. Subset size (39 x 39) and strain filter size (15) were used.

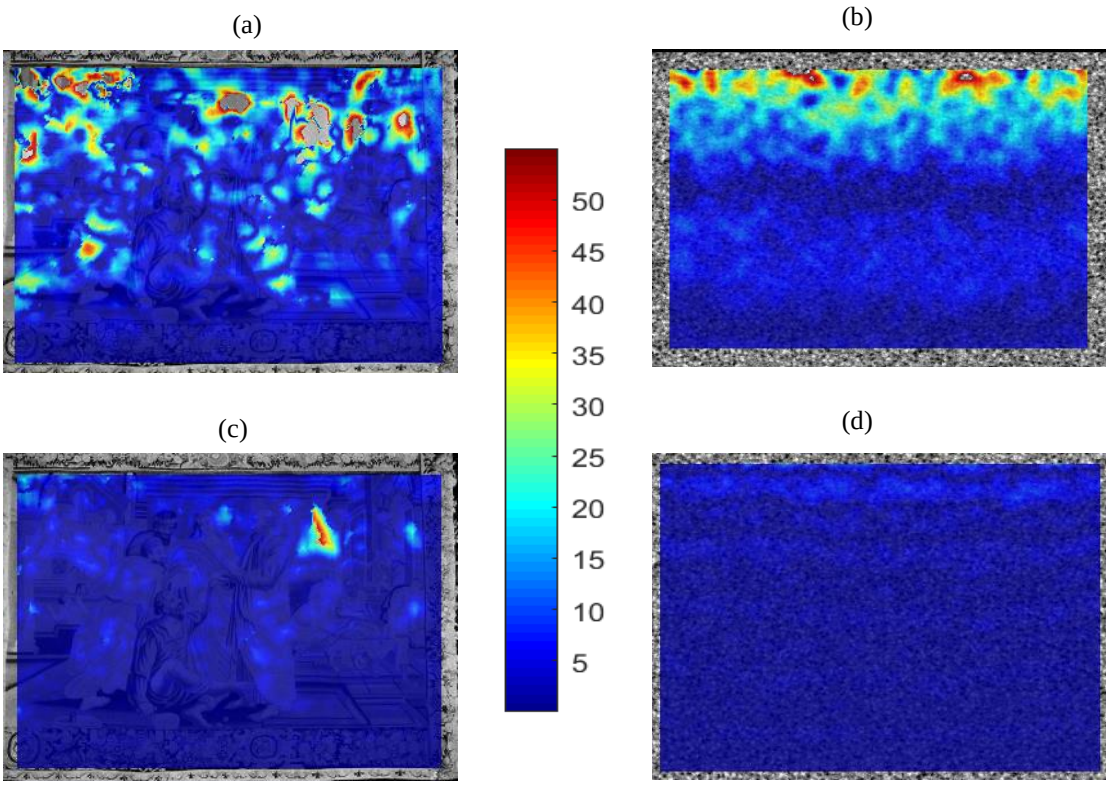

Fig. 8. Displacement field percent error map. (a) and (b) first load step (20% of imposed displacement) using tapestry and speckle images respectively. (c) and (d) last load step using tapestry and speckle images respectively. Subset size (39 x 39) and strain filter size (15) were used.

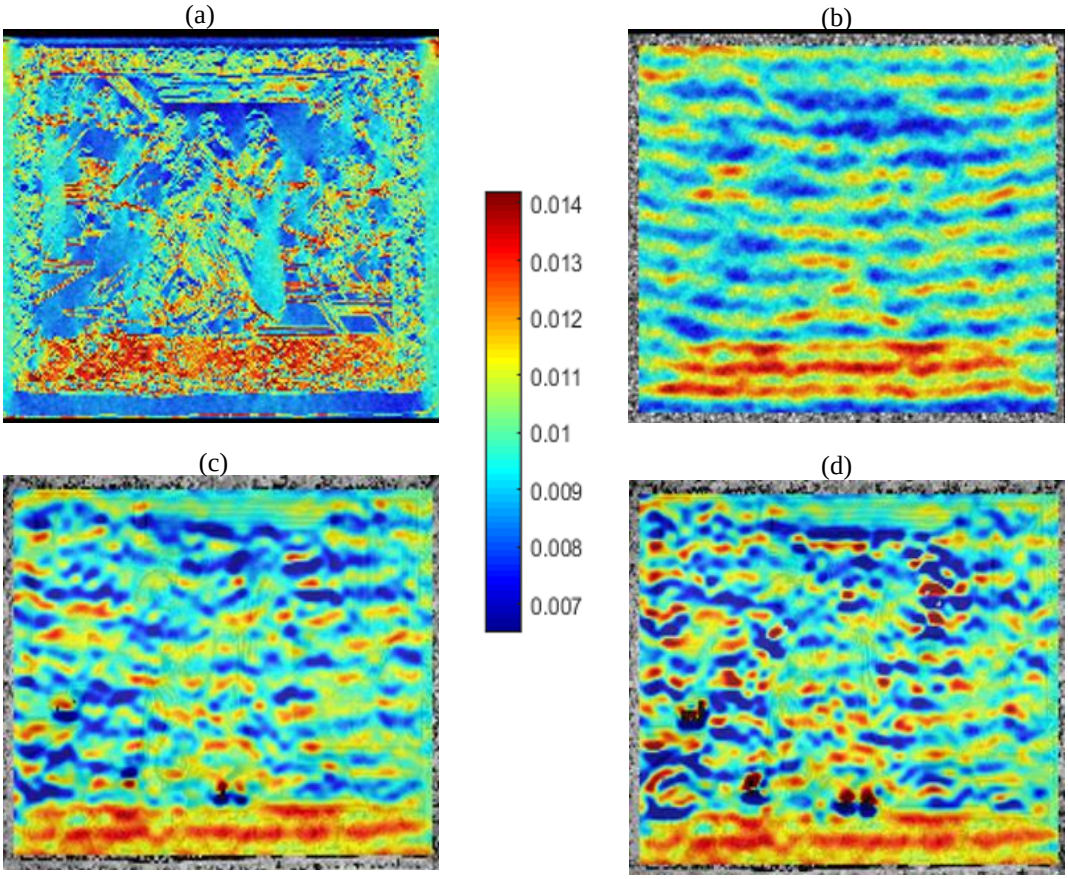

Fig. 9. Strain field. (a) FEA strain field interpolated on the tapestry image. (b) DIC predicted strain field with speckle image, (c) DIC predicted strain field with Tapestry 1 image using non-incremental correlation, (d) DIC predicted strain field with Tapestry 1 image using incremental correlation. Subset size (39 x 39) and strain filter size (15) were used.

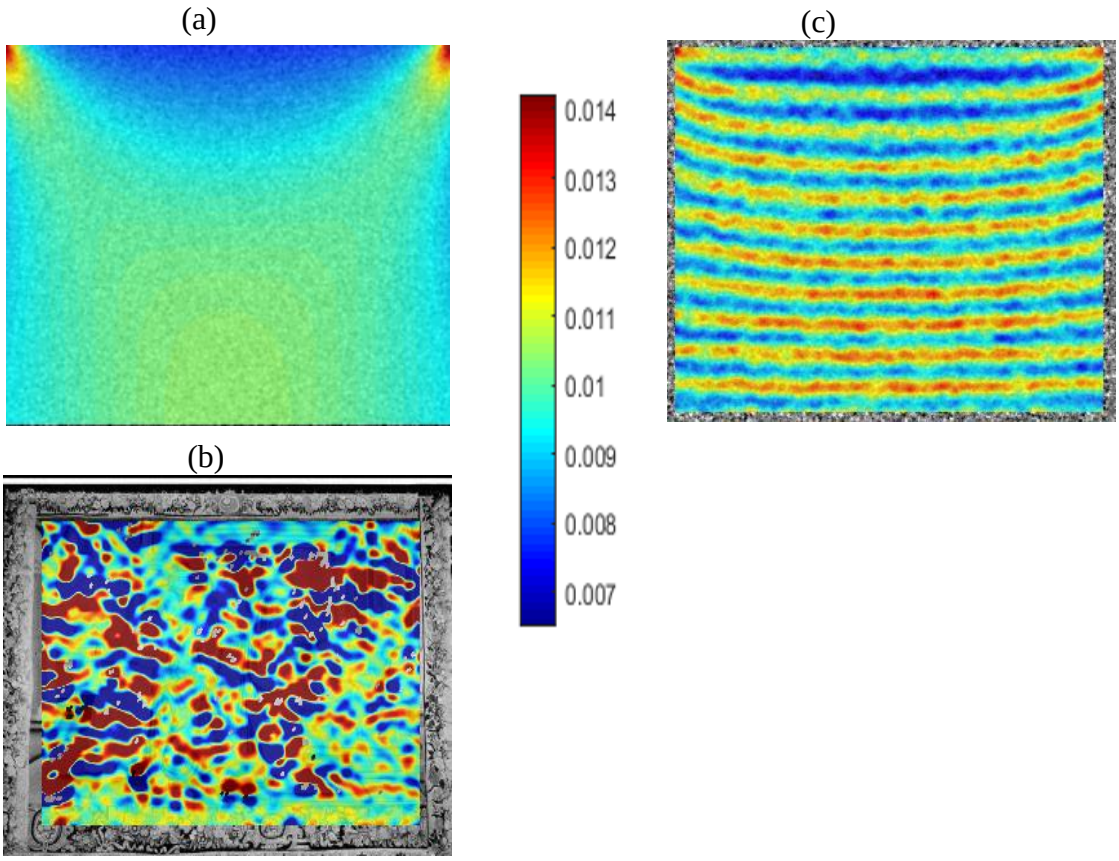

Fig. 10. Homogenous Strain field for 1% imposed strain: (a) FEA reference strain, (b) DIC with Tapestry 1 image, (c) DIC with speckle image. Subset size (39 x 39) and strain filter size (15) were used with non-incremental correlation.

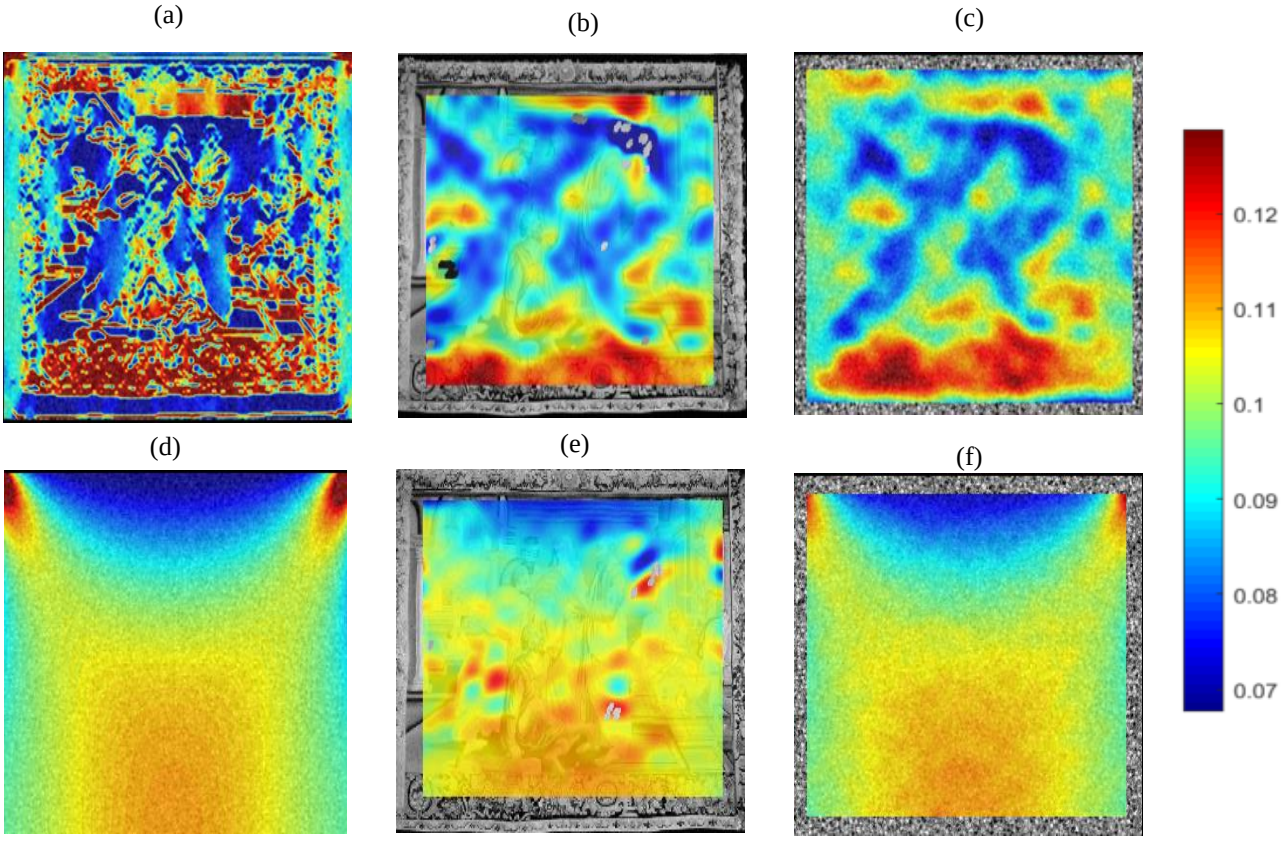

Fig. 11. 10% imposed strain field. Heterogenous strain field: (a) FEA reference strain, (b) DIC with Tapestry 1 image, (c) DIC with speckle image. Homogenous strain field:(d) FEA reference strain, (e) DIC with Tapestry 1 image, (f) DIC with speckle image. Subset size (39 x 39) and strain filter size (15) were used with non-incremental correlation.

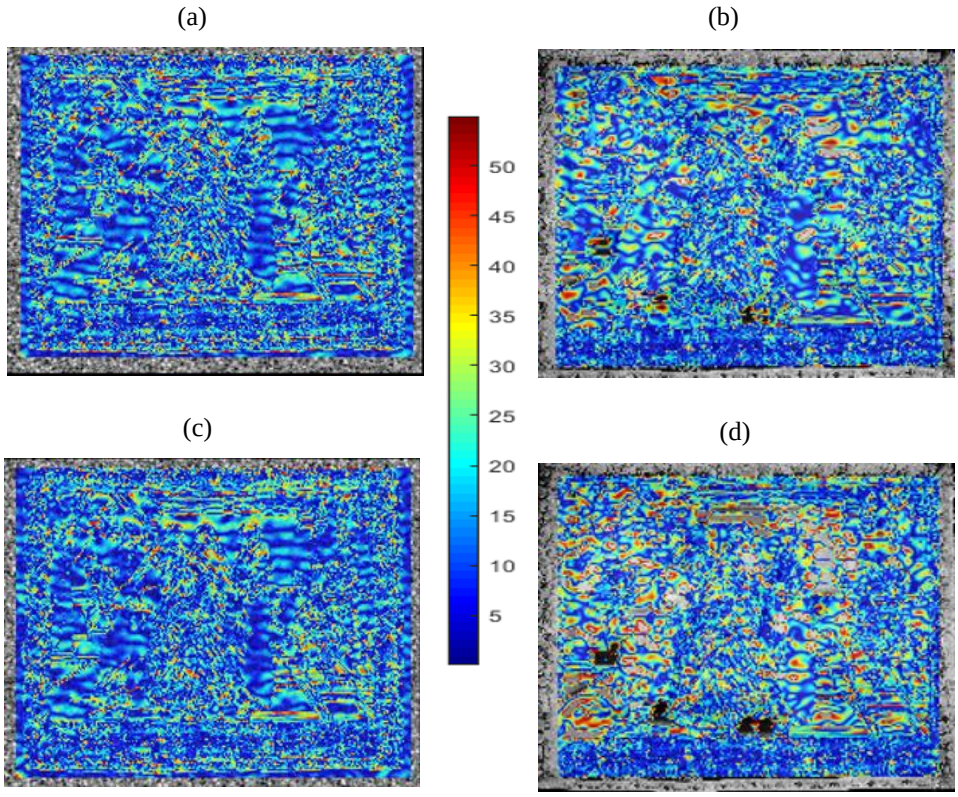

Fig. 12. Strain field percent error map. (a) speckle image with non-incremental correlation, (b) tapestry image with non-incremental correlation, (c) speckle image with incremental correlation, (d) tapestry image with incremental correlation.

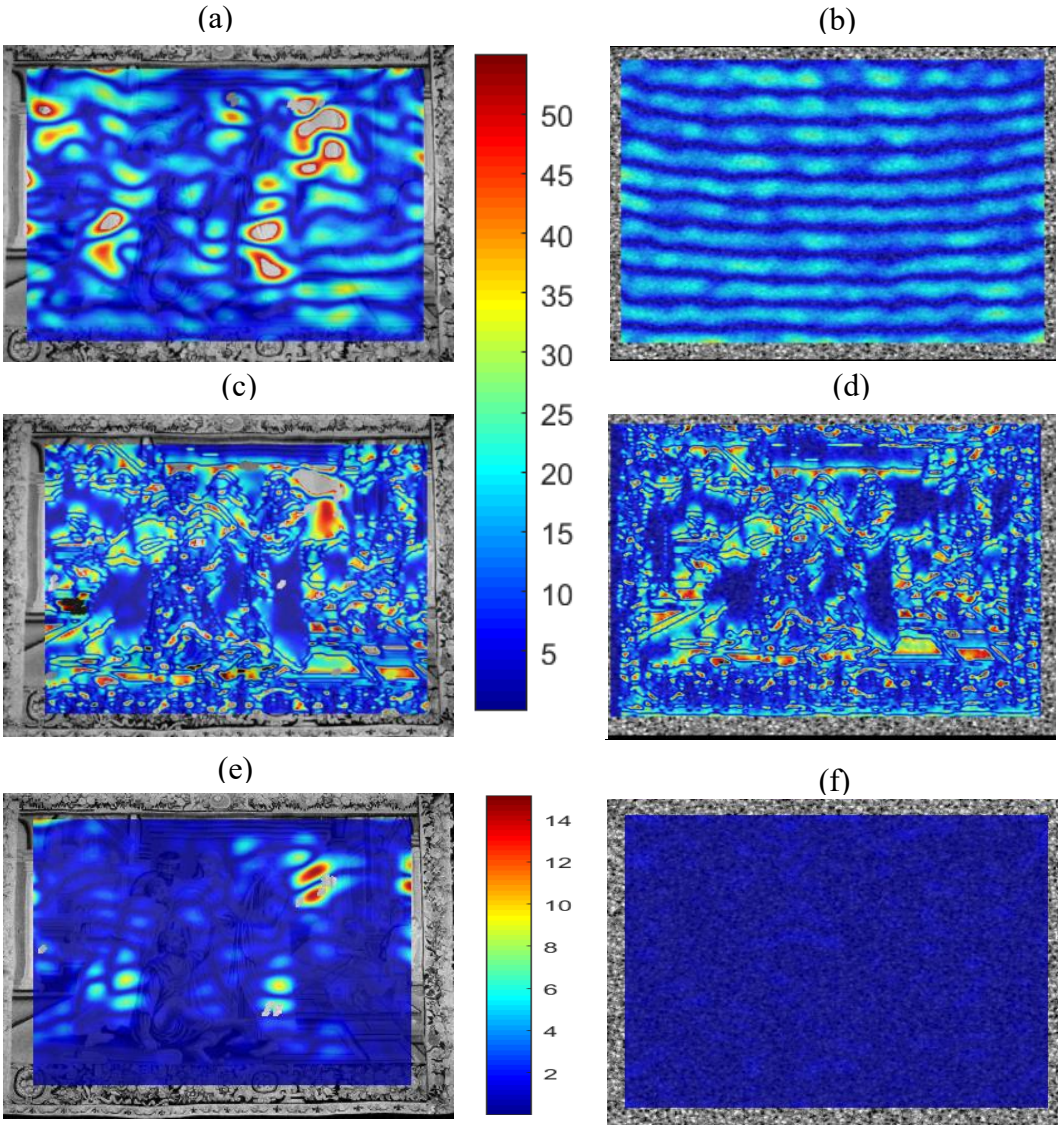

Fig. 13. Percent error maps. (a) tapestry 1 image and (b) speckle image at 1% strain level from homogenous strain field. (c) tapestry image and (d) speckle image at 10% strain level from heterogenous strain field. (e) tapestry image and (f) speckle image at 10% strain level from homogenous strain field. Subset size (39 x 39) and strain filter size (15) were used with non-incremental correlation.

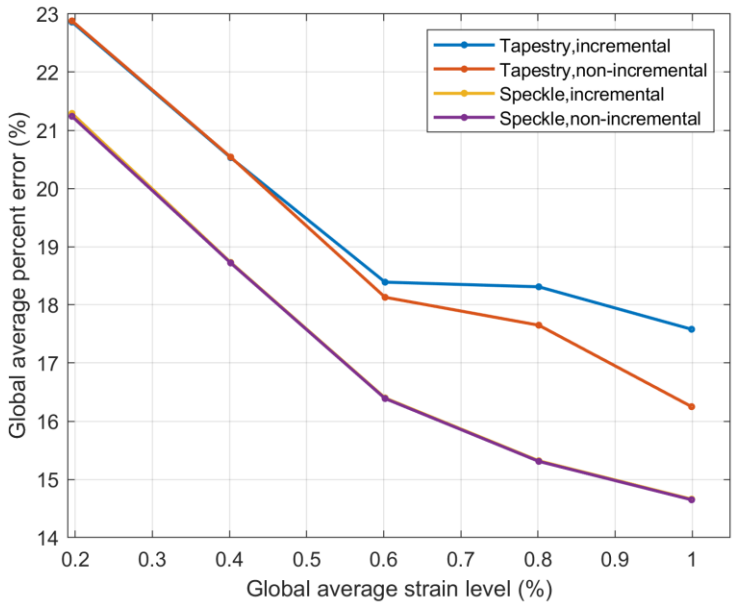

Fig. 14. Global average strain vs. global average percent error

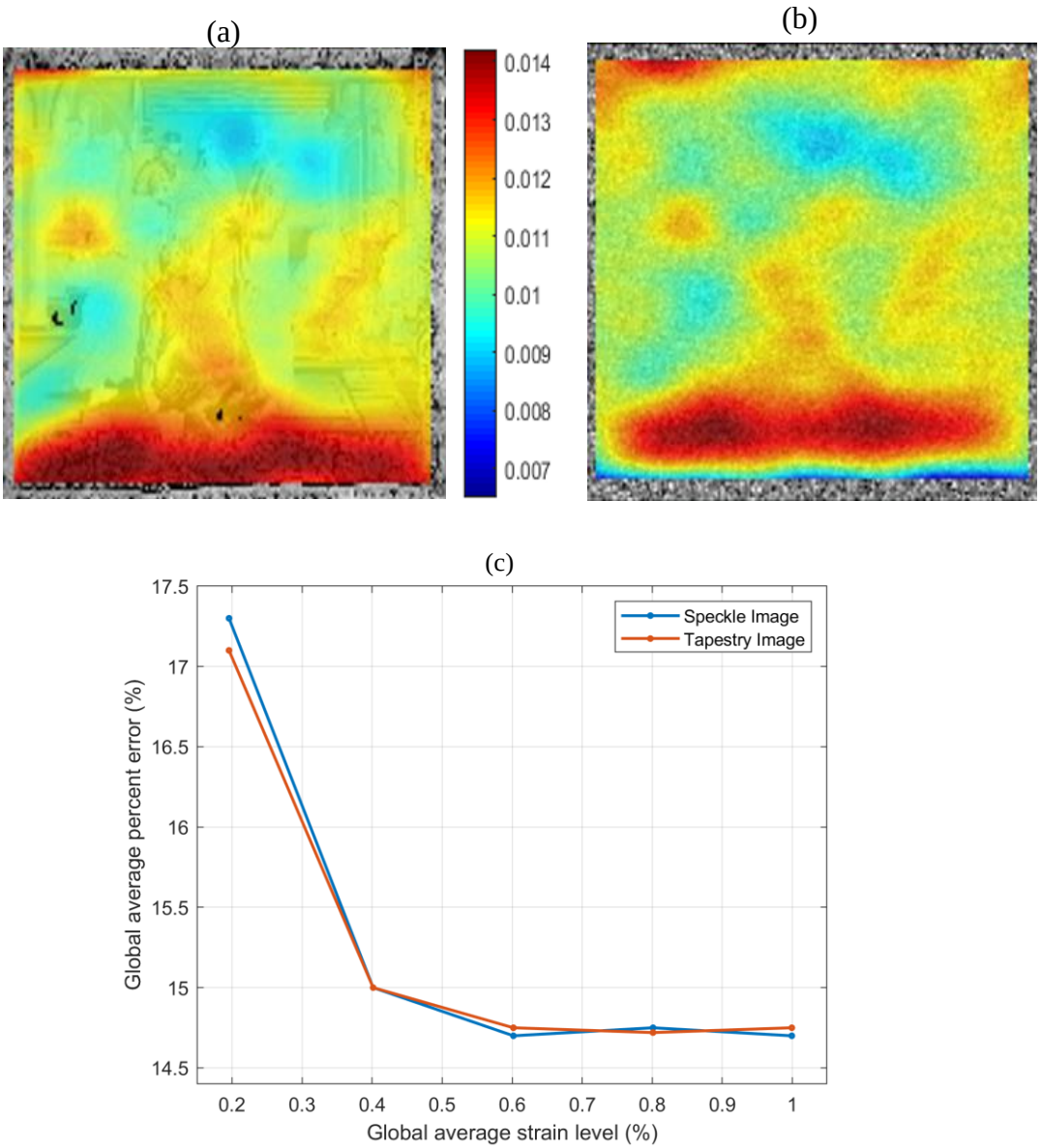

Fig. 15. DIC results with 59 strain filter size. (a) strain field with tapestry image, (b) strain field with speckle image and (c) global averaged percentage error vs global average strain. Subset size (39 x 39) with non-incremental correlation were used.

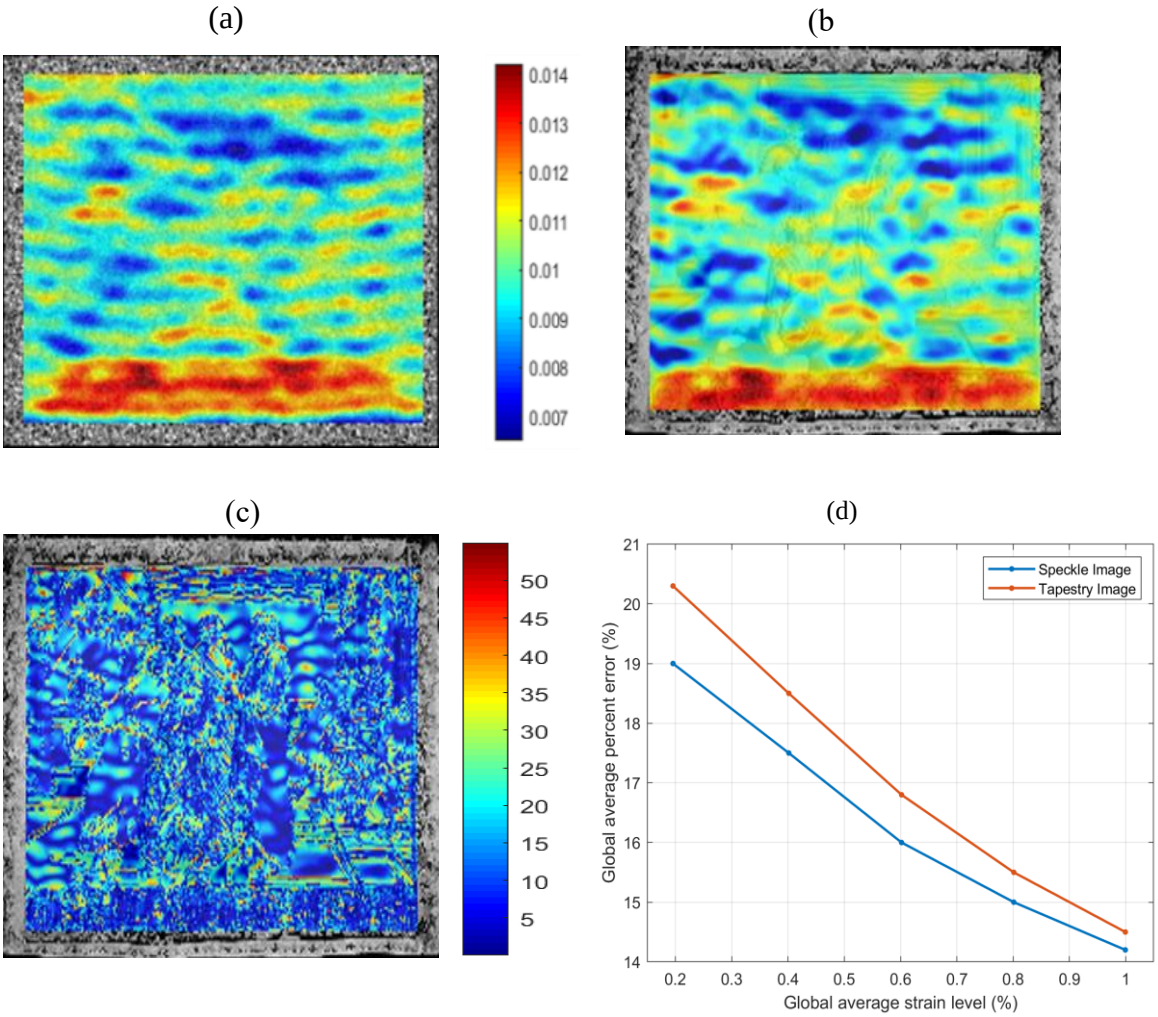

Fig. 16. DIC results with 79x79 subset size. (a) Strain field with speckle image. (b) strain field with tapestry image. (c) percent error map. (d) global average percent error vs. global average strain level. Strain filter size 15 with non-incremental correlation were used.

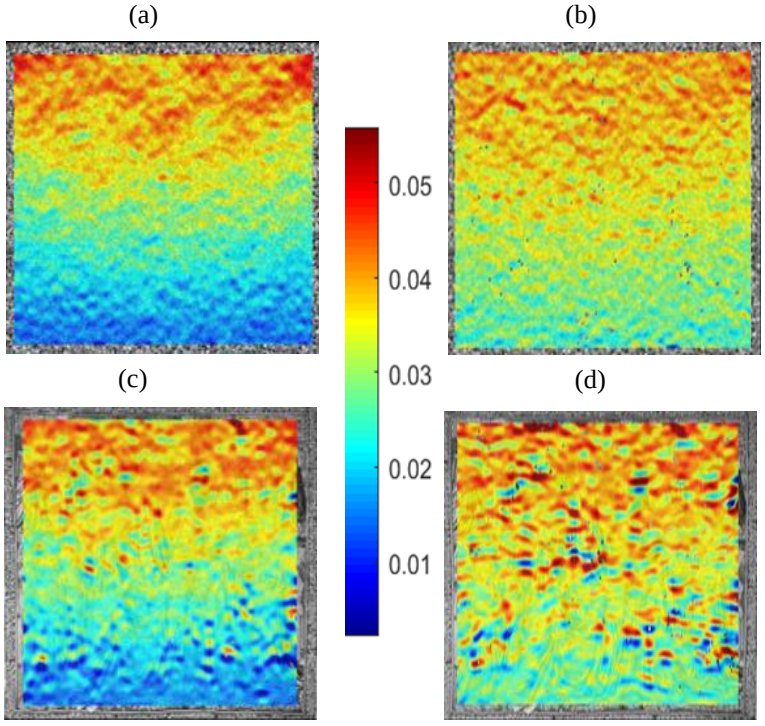

F*ig. 17. Strain field: (a) speckle image, half resolution, (b) speckle image, one-fifth resolution (c) tapestry image, half resolution, (d) tapestry image: one-fifth resolution. Subset size (39 x 39) and strain filter size (15) were used with non-incremental correlation.*

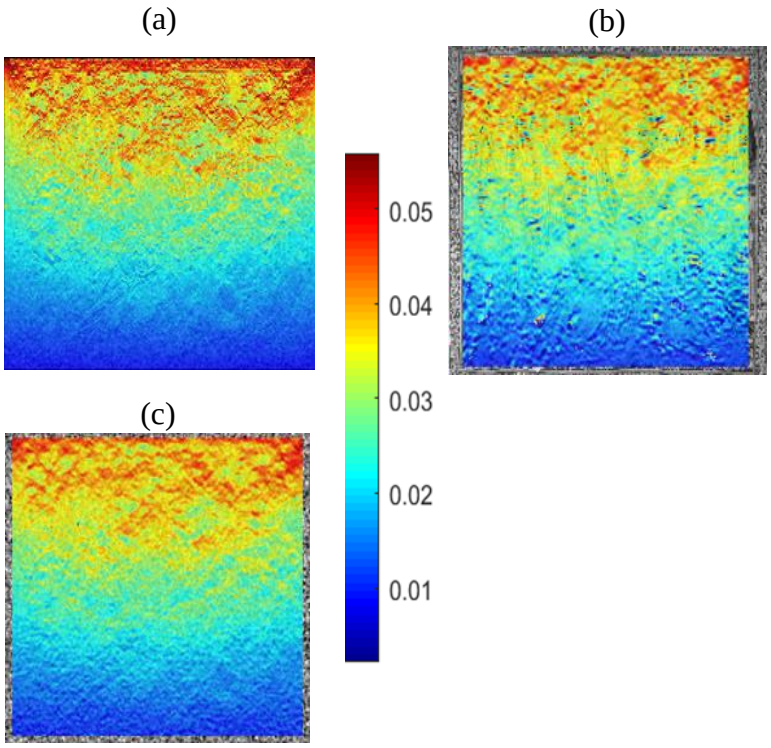

F*ig. 18. Strain field: (a) FEA strain reference field, (b) strain field from tapestry image 2 with original resolution (c) strain field from speckle pattern original resolution. Subset size (39 x 39) and strain filter size (15) were used with non-incremental correlation.*

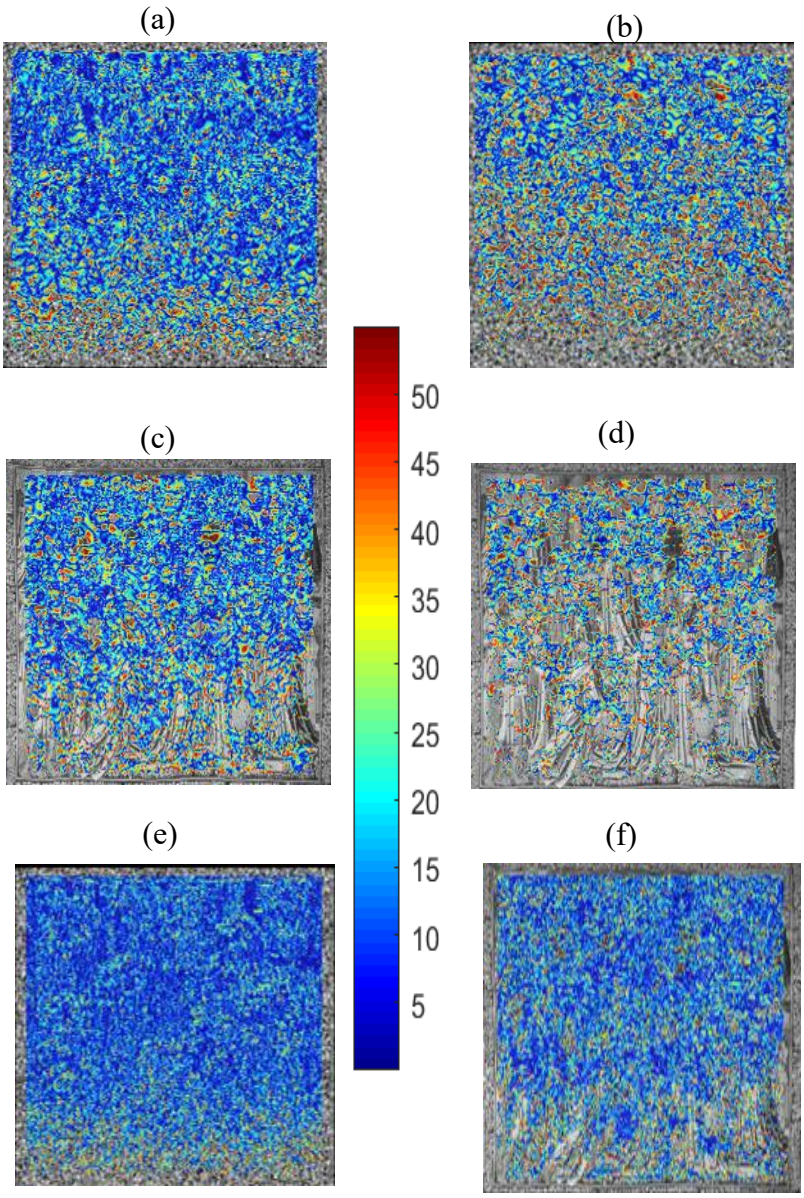

Fig.19. Percent error map: (a) speckle image, half resolution, (b) speckle image, one-fifth resolution, (c) tapestry image, half resolution, (d) tapestry image, one-fifth resolution, (e) original speckle pattern image, (f) original tapestry image.

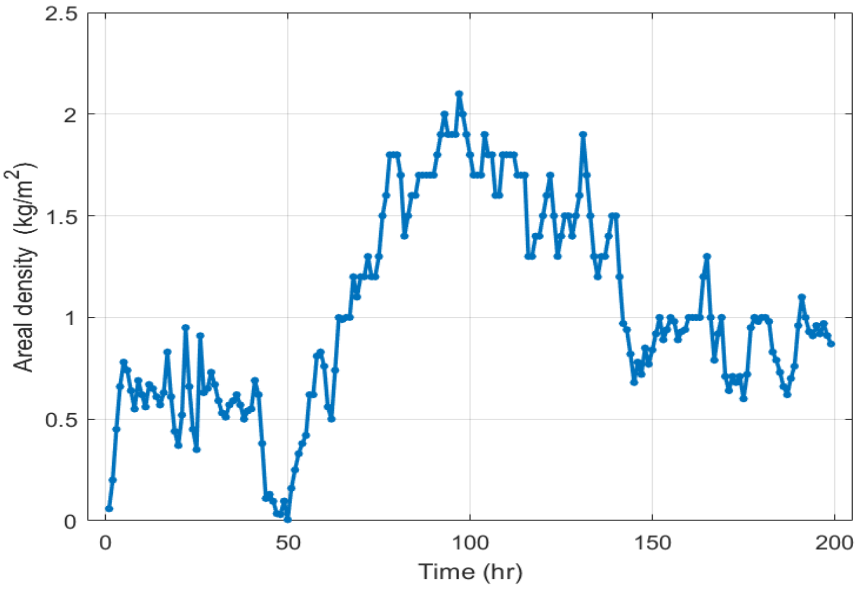

Fig. 20. Variation of areal density over time used for Case 3.

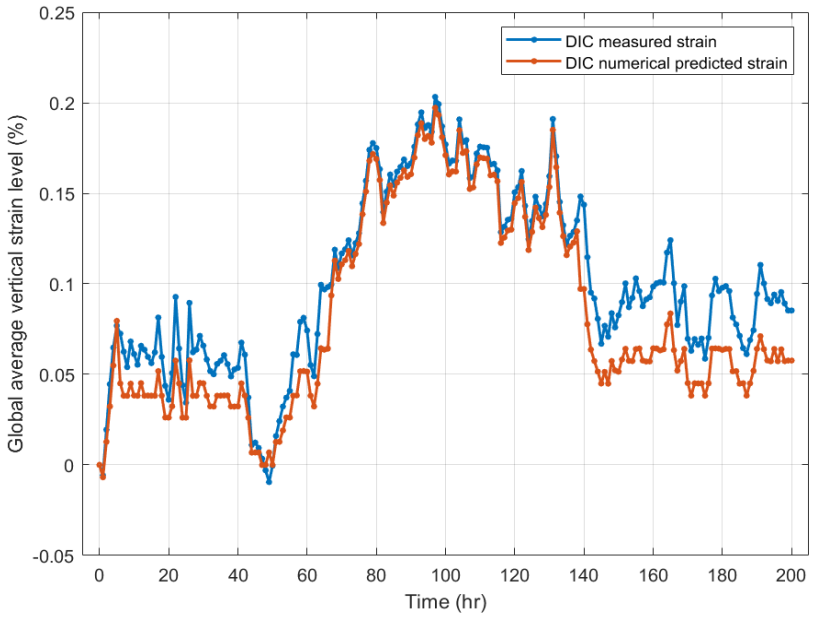

Fig. 21. Global averaged DIC measured strains and numerically imposed strains predicted by DIC.

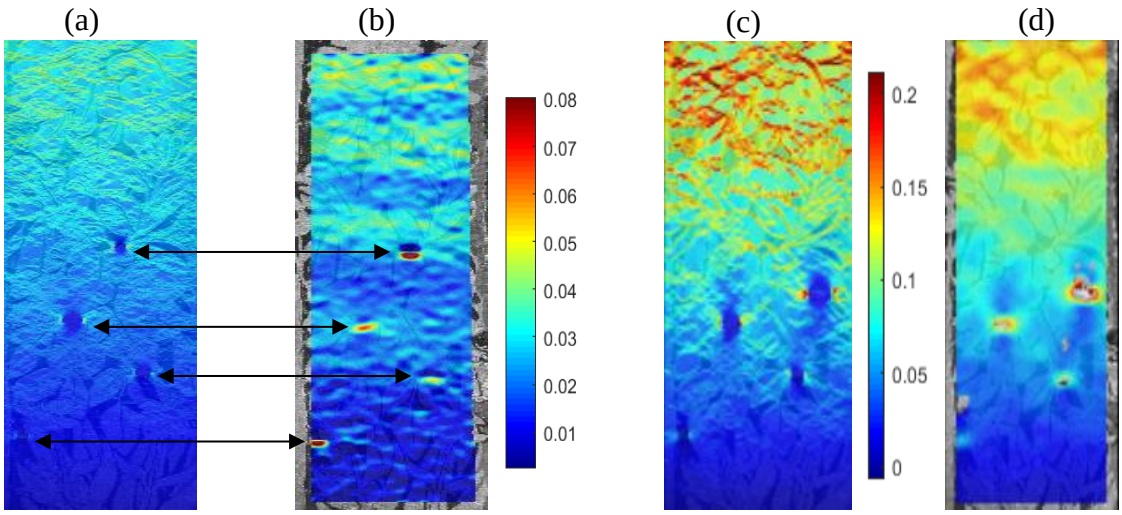

Fig. 22. Strain field showing the strain around the tears with the arrows showing the locations of corresponding tears. At 0.07% strain level: (a) from FEA, (b) DIC ROI using the tapestry fragment. The colour legend indicates the vertical component of strain. At 0.2% strain level: (c) from FEA, (d) DIC ROI using the tapestry fragment. The colour legend indicates the vertical component of strain. Subset size (39 x 39) and strain filter size (15) were used with non-incremental correlation.

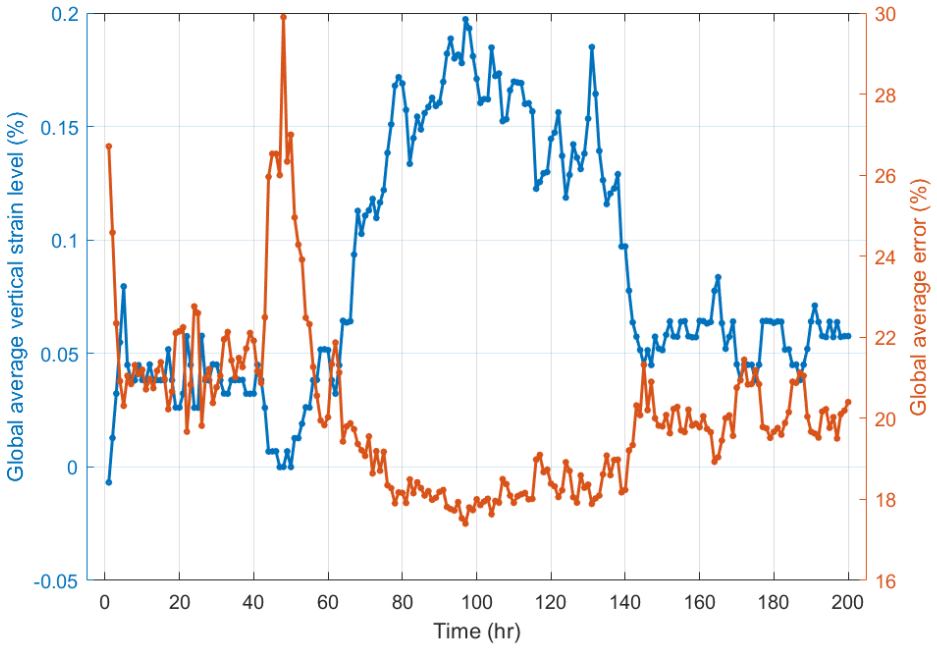

Fig. 23. Variation of average strain and percent error over time.

Tapestry type	Dimensions, Height x Width (mm)	Areal Density (Kgm^{-2})
1	N/A	0.9 (assumed)
2	3440 x 3980	0.9 (assumed)
3	1600 x 400	1.14 (measured)

Table 1. Details of tapestries used in the analyses.

Table 2: DIC Settings

Parameter	Definition
Subset size	The number of pixels in a 'subset' that carries unique gray scale value information required for tracking its displacement
Step size	Distance between the centre of each subset
Window size	Number of neighbouring subsets used in the calculation of a subset's strain value
Incremental correlation	Comparing the current deformed image with the previous deformed image to track displacement, i.e. the previous deformed image becomes the reference image for the correlation of the current deformed image
Direct correlation	Comparing each deformed image directly with the reference image in order to track displacement

Table 3: Image Quality

Parameter	Definition
Image resolution / size (a x b) pixels	The total number of pixels in the image
Image quality	Brightness (light/dark colour value), contrast (clear distinction between light and dark areas in an image for clear identification of details), noise

Table 4: Target image suitability

Parameter	Definition
Information density	Distribution of features on the image surface
Anisotropy	Distinct and random features
Repetition	An image containing one image repeating over and over could contain a lot of information and be isotropic but would be poor for DIC

Table 5. Global average percent error for different mesh densities

	Global percent error (%)	
Mesh density value	Speckle image	Tapestry image
5	13	18
10	10	15
20	6	11